Atomic Stacking Configurations in Atomic Layer Deposited TiN Films

Sean Li,* Z. L. Dong, B. K. Lim, M. H. Liang, C. Q. Sun, W. Gao, and H. S. Park

School of Materials Engineering, Nanyang Technological University, Singapore 639798

T. White

Institute of Environmental Science and Engineering, Singapore 637723

Received: August 22, 2002; In Final Form: October 10, 2002

Study on the atomic stacking configurations and grain boundary structures of ultrathin nanocrystalline TiN films deposited by the atomic layer deposition technique reveals that the dangling bonds and surface reconstruction may be the intrinsic factors that result in the crystal growth with different configurations. The surface topography of the amorphous SiO_2 layer is an extrinsic factor to affect the atomic stacking configurations in ultrathin nanocrystalline TiN films. The analysis indicates that the coherent boundary should be the favored boundary in the connection of the tilt grains. These atomic stacking and grain boundary configurations may be the main factors to produce the pinhole-free, high-density, and homogeneous ultrathin nanocrystalline TiN film prepared by the atomic layer deposition method. This study may provide new insight into the fundamental mechanism and properties of ultrathin TiN films.

Introduction

In Cu-based interconnects for ultra-large scale integration (ULSI) devices, the presence of Cu in silicon results in highly adverse effects, including the formation of deep trap levels that causes device degradation and failure.[1−3] TiN is one of the materials most commonly used as a diffusion barrier to prevent the Cu diffusion into Si and SiO_2.[4,5] A number of techniques including conventional chemical vapor deposition, physical vapor deposition, ionized metal plasma deposition, etc., have been employed to deposit high-quality diffusion barriers for the multilayer structure of the Cu-based interconnects. Since the structure of the ULSI devices has been scaled down to a deep submicron regime, the development of deposition technique is eagerly awaited to improve the step coverage of the diffusion barrier for next-generation devices. An atomic layer deposition (ALD) method is a promising technique for these applications because the saturation mechanism of ALD results in an inherent elimination of pinholes, excellent conformal coating characteristics, as well as good thickness uniformity and homogeneity of the thin film produced.[6−8] The applicability of ALD on the growth of TiN thin film has been successfully demonstrated.[8−10] Although the surface reaction and physical model of the atomic layer deposition in the process have been systematically studied,[6,11−13] the atomic stacking configurations and the grain boundary structures of ultrathin TiN film deposited by ALD technique are still not clear. Study on the atomic stacking configuration and grain boundary structure will reveal the actual mechanism of the TiN film formation in the ALD process and the dominating factors which determine the film growth and its reliability as a diffusion barrier.

Experiment

A 300 nm SiO_2 layer was deposited on a Si substrate using PECVD, and subsequently a 30 nm TiN film was deposited on the SiO_2 by ALD technique in a Pulsar 2000 reactor with pure precursors of $TiCl_4$ and NH_3 at 390 °C in N_2 purging gas. Finally, a 350 nm Cu film with column grain structure was deposited on the TiN layer by magnetron sputtering deposition to obtain the Cu/TiN/SiO_2/Si structure. The atomic stacking configurations, interfacial characteristics, and grain boundary structure of the ultrathin TiN film in the structure were investigated by high-resolution transmission microscopy (HRTEM). The cross-sectional HRTEM samples were prepared with the conventional "sandwich" technique.

Results and Discussion

TEM morphology in Figure 1a shows that a homogeneous ultrathin TiN layer with high density was deposited on the amorphous SiO_2 layer by the ALD method. A number of TiN(111) and (200) lattice fringes in Figure 1b, a HRTEM image, reveals that the as-deposited TiN layer consisted of ∼5 nm nanocrystals, which mainly grew with atomic stacking on the TiN(111) and (200) planes on the SiO_2 surface. The interfacial characteristic in Figure 1b also shows that the surface topography of the amorphous SiO_2 layer was not flat in nanoscale. In general, the maximum density of the atoms in the monatomic layer, which is defined as a surface configuration formed by add-atoms directly bonded to the underlying surface during the ALD process,[11] is a close-packed configuration with minimum free energy. TiN has a face-center cubic structure and (111) is its close-packed plane. Based on the physical model of the atomic layer deposition, the epitaxy single-crystal film that the close-packed crystalline planes parallel to the surface should, in theory, form during the ALD process.[6] However, the chemistry of the surface reactions is far more complicated than simply laying atomic layers on top of each other. A surface always creates a discontinuity of the bulk which means that either there are dangling bonds on the surface or the unsaturated bonds are terminated by surface reconstruction, etc.[11] The dangling bonds on the surface and the surface reconstruction

* Corresponding author. E-mail: assxli@ntu.edu.sg.

10.1021/jp026814e CCC: $22.00
Published on Web 11/07/2002

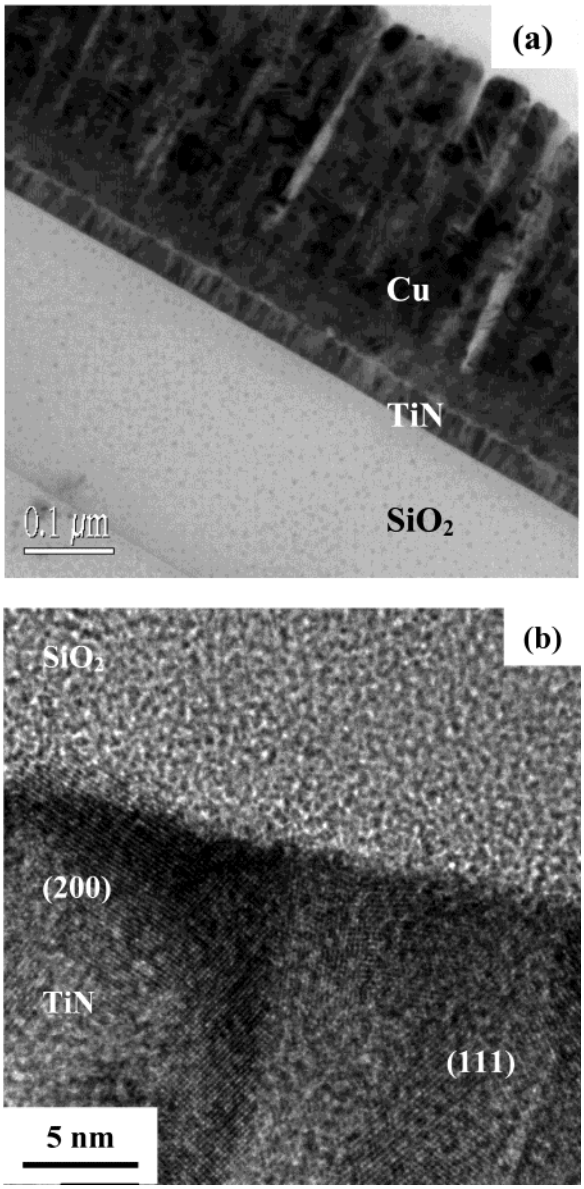

Figure 1. (a) TEM morphology showing a high-density and homogeneous ultrathin TiN layer deposited on the surface of an amorphous SiO_2 layer by ALD technique. (b) HRTEM image exhibits that the as-deposited TiN layer has nano-polycrystalline characteristics but the layer was formed mainly by atomic stacking along TiN close-packed plane (111) and plane (200) from the SiO_2 surface.

may result in the structure of the initial as-deposited monatomic layer deviating from the ideally close-packed configuration. In this case, the subsequent atom stacking on the previously deposited monatomic layer may result in two crystal structures: (1) The atom stacking may eliminate the dangling bonds in the underlying monatomic layer, producing an epitaxial layer with close-packed density; and (2) The subsequently deposited atoms may just simply lie on the top of the reconstructed monatomic layer, forming an epitaxial film with a heredity density lower than the close-packed density, such as TiN(200) configuration. These may be one reason the lattice fringes of the close-packed planes (111) and planes (200) were frequently observed in the cross-sectional HRTEM morphology of the ultrathin TiN film. In most cases, the ideal saturation (close-packed) density for a full monatomic layer is not easy to achieve because of surface reconstruction.[6] This may result in the variation of atomic stacking features intrinsically during the film growth, thus producing nano-polycrystalline structure.

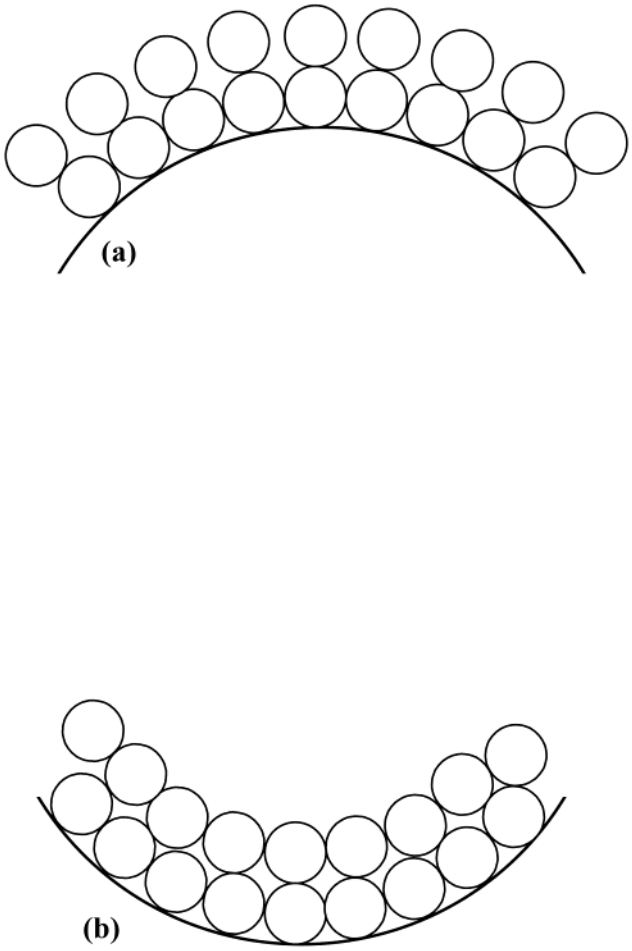

Figure 2. Schematic showing the density variation of a monatomic layer deposited on (a) a convex surface, and (b) a concave surface of the amorphous SiO_2 layer.

On the other hand, the atomic stacking features are also strongly influenced by the surface topography of the substrate. From the physical model of the ALD process,[11] it can be inferred that the ideally close-packed density of the monatomic layer can only be achieved on a planar surface. Figure 2 is a schematic of the atomic configuration. If the atoms deposited on a convex surface of the substrate with the saturation density (Figure 2a), the atomic packing density in the subsequently deposited monatomic layer would be lower than the close-packed density, such as the density of (200) planes. In contrast, if the atoms deposited on a concave surface (Figure 2b), the atomic packing density on the deposited monatomic layer surface should be greater than the close-packed density. In the later case, the subsequently deposited atoms cannot lie on the utmost top of the corresponding atom positions because of the congested space on the surface of the monatomic layer. Therefore, no epitaxy film can form.

It is proposed that the curvature of the surface of the substrate plays an important role in determining the orientation of the crystal growth and the atomic stacking feature. Figure 3 shows the TiN/SiO_2 interfacial characteristics. A SiO_2 protuberance with a large curvature is observed (arrowed with A). It can be clearly seen that the lattice fringes of TiN(200) (arrowed with B and C) are parallel to the slope facets of the convex surface while the lattice fringes of the neighbor crystal (arrowed with D) are parallel to the bottom facet beside the protuberance.

Figure 4a shows the atomic stacking feature of a crystal that was deposited on a convex surface with a smaller curvature. It

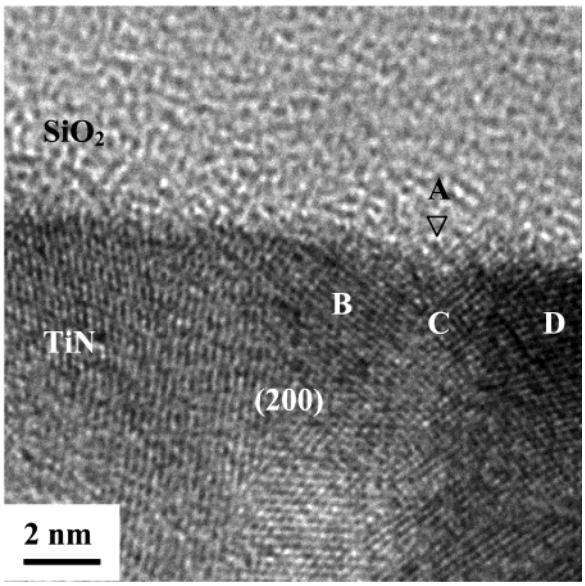

Figure 3. HRTEM morphology showing the TiN/SiO_2 interfacial characteristics and the crystal orientation of TiN around the hump of SiO_2.

shows that the film grew epitaxially in the first 10 monatomic layers stacking on (200) planes (marked by A) and then split into two crystals marked by B and C, respectively. Geometrically, the surface of any two-dimensional convex surface with a small curvature can be resolved into two planar facets with a very small misorientation. The crystals, therefore, grew epitaxially on these planar facets, respectively. In the first few atomic deposition cycles, the effects of such a small misorientation on film growth is negligible. The gap between the crystals was so small that it could be neglected, exhibiting a pseudo-epitaxy growth characteristic with multi-monatomic layers, until the size of the gap was comparable with the size of the TiN atom, as shown in Figure 4a. In fact, the gap between crystals B and C in the 11th monatomic layers of the crystals is discernible. Since the gap is smaller than the diameter of the atom, atoms cannot fill the gap to form a continuous (200) pseudo-monatomic layer. Hence, a discontinuous layer is formed. In the subsequent deposition cycle, the deposited atoms lie on the top of the 11th atomic layer to form the epitaxy 12th discontinuous atomic layer.

For the gap, two configurations are possible in the subsequent deposition. If the gap is small enough, the atoms may either simply lie in it or just leave it open. The open gap can be clearly seen from the 15th to 18th atomic layers (arrowed with X) while an atom lies on the site of the gap space in the 19th atomic layer (arrowed with Y), resulting in the changes of the atom stacking configuration in the subsequent deposition cycles. For example, the atoms on the 20th atomic layer in crystal C lie in the space between the atoms instead of on top, producing stacking faults till an atom is partially inserted into the gap of the 22nd atomic layer (arrowed with Z). In the subsequent deposition cycles, the (200) planes in crystals B and C are no longer on the same level, and the atoms start to fill the gap space disorderly. It is difficult to define the structure of the gap between the two crystals, although the atoms in the gap can be clearly discerned. It is probably a transitional structure with a semicrystalline character that has a considerably high density. This atom stacking feature dominates with further deposition giving rise to the formation of two columns of crystals B and C based on the pseudo-epitaxy "complex" of crystal A.

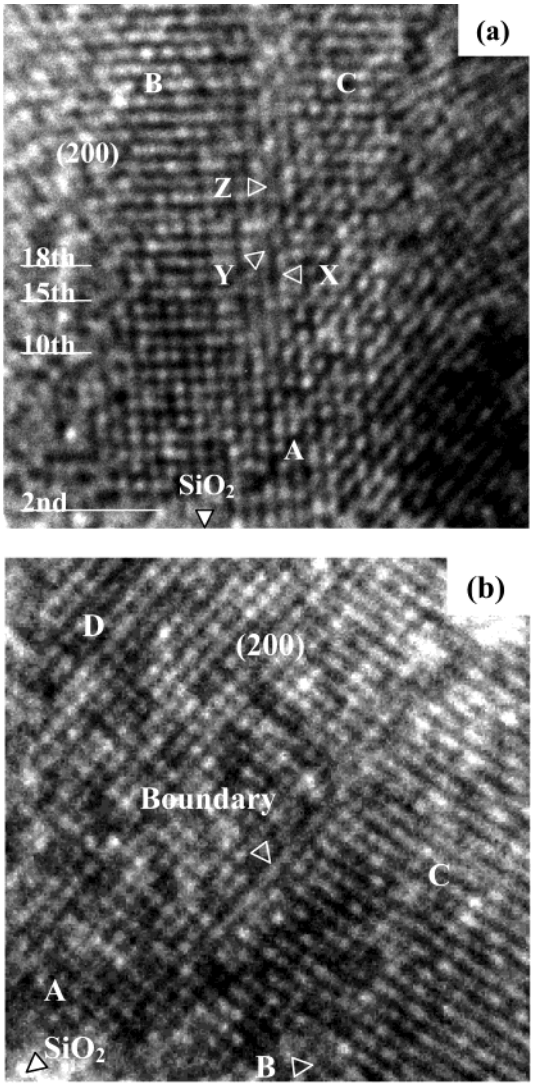

Figure 4. (a) HRTEM image showing the variation of the atomic stacking configurations. (b) HRTEM image showing that the stacking fault varied the orientation of the atomic layers, splitting one crystal into two.

Despite the effect of surface topography, the atomic stacking fault also strongly influences the orientation of the epitaxy crystals grown by ALD technique. Figure 4b shows a lattice image of the crystals deposited by ALD technique. The film grew epitaxially in the first 10 (200) atomic layers (marked by A). An incomplete (half) atomic layer (arrowed with B) can be seen to form on the 10th atomic layer. Subsequent layers with (200) configuration (marked by C) above this incomplete atomic layer grew epitaxially with a small tilted angle of 7° to the (200) monatomic layers in crystal D. This led to the formation of crystals C and D from the pseudo-epitaxy "complex" of crystal A with different orientations. It may be another mechanism that the nano-polycrystalline structure formed during the ALD process. The small-angle grain boundary between crystals C and D is a strain-free coherent boundary because the (200) planes of both crystals connected each other at the boundary.

However, large-angle grain boundaries are frequently observed in the ALD film. Figure 5a shows a high-resolution morphology of a grain boundary between the crystals (crystals A and B) with a 30° misorientation of TiN(111) planes. This boundary consisted of three regions with different characteristics marked by X, Y, and Z, respectively. Since the (111) lattice fringes of crystal B terminated on the (111) lattice fringes of

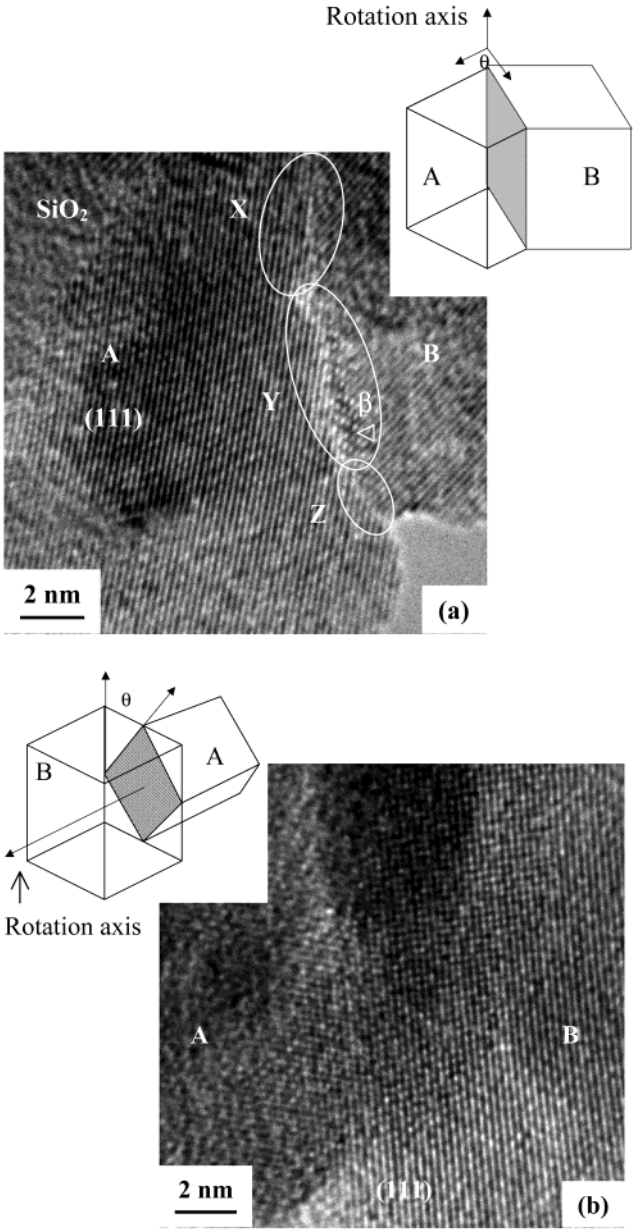

Figure 5. (a) HRTEM image showing that the grain boundary consists of three regions with different structures, i.e., incoherent boundary, transition structure, and coherent boundary, with the low-energy strain-free coherent boundary as a favored boundary for the tilt grains. The inset is a schematic illustration of the tilt grain boundary. (b) HRTEM image showing a twist grain boundary in the ultrathin TiN film. The inset is a schematic of the twist grain boundary.

crystal A with 30° in region X, the boundary in this region is incoherent. However, the (111) lattice fringes of crystals A and B connected each other in region Z, exhibiting the characteristic of a strain-free coherent boundary. The boundary structure of region Y is complex, and it is a transitional region from incoherent to coherent boundary structures. The atomic image (arrowed with β) shows that atoms in this transitional region are self-organized to adjust their positions to fit the structural change. Figure 5a also shows that the grain boundary formed in the order of first incoherent boundary, then transitional structure and coherent boundary from the TiN/SiO_2 interface to TiN surface. It implies that the low-energy strain-free coherent boundary is a favored boundary for the tilt crystals (inset in Figure 5 a) in the film deposited by ALD technique, although the tilt crystals nucleate with different orientations. This phenomenon may be related to the growth energy of the monatomic layer. In Figure 5a, it can be clearly seen that the width of the boundaries is in an atomic scale regardless of what structures the grain boundaries have. This kind of atomic scale boundary can effectively restrict the boundary diffusion, which is the major interdiffusion mechanism in semiconductor devices. However, the other type of boundary, such as twist boundary, can also be observed in the film deposited by ALD technique. Figure 5b shows the (111) lattice fringes of two TiN grains partially overlapped, evidence of the twist boundary.

Conclusion

The atomic stacking configurations and grain boundary structures in the TiN film deposited by ALD technique are studied in detail. The result shows that the ultrathin TiN film consists of nano crystals, which mainly grew with atomic stacking on the TiN (111) and (200) planes. The bond dangling and surface reconstruction may be the intrinsic mechanism to cause the crystals to grow with different configurations. However, the surface topography of the amorphous substrate is an extrinsic mechanism to dominate the atomic stacking configurations, thus resulting in the nano-polycrystalline structure in the film. Evidence shows that some of the epitaxy crystals split into two crystals because of the geometry of the amorphous substrate surface or the stacking faults induced by the ALD process. The tilt and twist grain boundaries with the width in atomic scale were observed in the film, and the coherent boundary should be the favored boundary in the connection of the tilt grains. These atomic stacking and grain boundary characteristics should be the dominant factors to produce the pinhole-free, high-density, and homogeneous ultrathin polycrystalline TiN film.

References and Notes

(1) Torres, J. *Appl. Surf. Sci.* **1995**, *91*, 112.
(2) Broniatowski, A. *Phys. Rev. Lett.* **1989**, *62* 3074.
(3) Sze, S. M. *Semiconductor Devices, Physics and Technology*; Wiley: New York, 1985.
(4) Kaloyeros, A. E.; Eisenbraun, E. *Annu. Rev. Mater. Sci.* **2000**, *30*, 363.
(5) Kumar, A.; Bakhru, H.; Jin, C.; Lee, W. W.; Lu, T.-M. *J. Appl. Phys.* **2000**, *87*, 3567.
(6) Suntola, T. *Thin Solid Films* **1992**, *216*, 84.
(7) Ritala, M.; Leskelä, M. *Nanotechnology* **1999**, *10*, 19.
(8) Ritala, M.; Leskelä, M.; Dekker, J.; Mutsaers, C.; Soininen, P. J.; Skarp, J. *Chem. Vap. Deposition* **1999**, *5*, 7.
(9) Juppo, M.; Ritala, M.; Leskelä, M. *J. Electrochem. Soc.* **2000**, *147*, 3377.
(10) Jeon, H.; Lee, J. W.; Kim, Y. D.; Kim, D. S.; Yi, K. S. *J. Vac. Sci. Technol. A* **2000**, *18*, 1595.
(11) Suntola, T. *Appl. Surf. Sci.* **1996**, *100/101*, 391.
(12) Goodman, C. H. L.; Pessa, M. V. *J. Appl. Phys.* **1986**, *60*, R65.
(13) Leskelä, M.; Ritala, M. *J. Phys. IV France* **1999**, *9*, Pr8−837.